A Halomethane Thermochemical Network from iPEPICO Experiments and Quantum Chemical Calculations
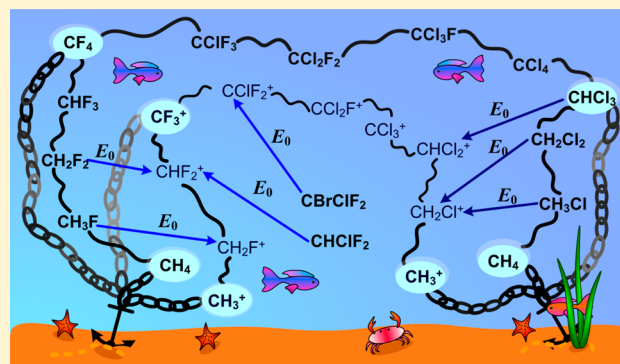
Jonelle Harvey,[†] Richard P. Tuckett,*,[†] and Andras Bodi*,[‡]

[†]School of Chemistry, University of Birmingham Edgbaston, Birmingham, B15 2TT, U.K.

[‡]Molecular Dynamics Group, Paul Scherrer Institut, CH-5232 Villigen, Switzerland

S *Supporting Information*

ABSTRACT: Internal energy selected halomethane cations CH_3Cl^+, $CH_2Cl_2^+$, $CHCl_3^+$, CH_3F^+, $CH_2F_2^+$, $CHClF_2^+$, and $CBrClF_2^+$ were prepared by vacuum ultraviolet photoionization, and their lowest energy dissociation channel studied using imaging photoelectron photoion coincidence spectroscopy (iPEPICO). This channel involves hydrogen atom loss for CH_3F^+, $CH_2F_2^+$, and CH_3Cl^+, chlorine atom loss for $CH_2Cl_2^+$, $CHCl_3^+$, and $CHClF_2^+$, and bromine atom loss for $CBrClF_2^+$. Accurate 0 K appearance energies, in conjunction with ab initio isodesmic and halogen exchange reaction energies, establish a thermochemical network, which is optimized to update and confirm the enthalpies of formation of the sample molecules and their dissociative photoionization products. The ground electronic states of $CHCl_3^+$, $CHClF_2^+$, and $CBrClF_2^+$ do not confirm to the deep well assumption, and the experimental breakdown curve deviates from the deep-well model at low energies. Breakdown curve analysis of such shallow well systems supplies a satisfactorily succinct route to the adiabatic ionization energy of the parent molecule, particularly if the threshold photoelectron spectrum is not resolved and a purely computational route is unfeasible. The ionization energies have been found to be 11.47 ± 0.01 eV, 12.30 ± 0.02 eV, and 11.23 ± 0.03 eV for $CHCl_3$, $CHClF_2$, and $CBrClF_2$, respectively. The updated 0 K enthalpies of formation, $\Delta_f H^{\circ}_{0K}(g)$ for the ions CH_2F^+, CHF^+, $CHCl_2^+$, CCl_3^+, CCl_2F^+, and $CClF_2^+$ have been derived to be 844.4 ± 2.1, 601.6 ± 2.7, 890.3 ± 2.2, 849.8 ± 3.2, 701.2 ± 3.3, and 552.2 ± 3.4 kJ mol^{-1}, respectively. The $\Delta_f H^{\circ}_{0K}(g)$ values for the neutrals CCl_4, $CBrClF_2$, $CClF_3$, CCl_2F_2, and CCl_3F and have been determined to be −94.0 ± 3.2, −446.6 ± 2.7, −702.1 ± 3.5, −487.8 ± 3.4, and −285.2 ± 3.2 kJ mol^{-1}, respectively.

1. INTRODUCTION

Quantum chemical calculations on small molecules can result in thermochemical values with a few kilojoules per mole uncertainties or better, often outperforming experimental results.[1−5] Recent threshold photoelectron photoion coincidence (TPEPICO) experiments, in which both the photon and the photoelectron energies are known to within 1−2 meV (0.1−0.2 kJ mol^{-1}),[6−9] are capable of measuring dissociative photoionization onset energies in small to medium sized molecules with such levels of accuracy. In the absence of an overall reverse barrier, the onset energies, E_0, correspond to the reaction energy at 0 K, and yield the enthalpies of formation for the parent ion, daughter ion, or neutral fragment if two out of the three are known:

$$E_0 = \Delta_f H_{0K}[\text{ion}] + \Delta_f H_{0K}[\text{neutral fragment}]$$
$$- \Delta_f H_{0K}[\text{neutral parent molecule}] \quad (1)$$

Recent advances in ab initio methods can be rigorously tested and confirmed by experimental techniques. The two approaches are, thus, complementary and can be applied simultaneously to provide sturdier results. For example,

inspired by the W3 and HEAT protocols,[10,11] highly accurate enthalpies of formation have been derived by Csontos et al.[3] for a comprehensive range of neutral halogenated methanes, although some of their results still need to be confirmed.

In TPEPICO, unimolecular dissociation reactions of internal energy selected parent ions are studied as a function of photon energy, yielding daughter ion appearance energies.[12] Ions are mass analyzed in delayed coincidence with threshold electrons, and the breakdown diagram is generated by plotting the fractional abundance of parent and fragment ions as a function of $h\nu$. For a fast dissociation, every parent ion with more internal energy than the dissociation threshold results in a fragment ion, and the breakdown curve of the parent ion corresponds to the cumulative distribution function (CDF) of the ion internal energy to the dissociation energy. In the first approximation, it follows that the breakdown curve corresponds to the CDF of the internal energy of the neutral at the experimental temperature

$$BD(h\nu) = \int_0^{E_0-IE} P_i(E,h\nu)\,dE \cong \int_0^{E_0-h\nu} P_n(E)\,dE \qquad (2)$$

where P_i is the normalized internal energy distribution of the parent ion as a function of the internal and photon energies. P_n is the internal energy distribution of the neutral molecule, calculated using the Boltzmann formula $P_n(E) = \rho_n(E) \cdot e^{-E/kT}$, where $\rho_n(E)$ is the density of states of the neutral.

The above integral vanishes at $h\nu = E_0$. Consequently, the 0 K appearance energy, E_0, is given by the disappearance energy of the parent ion in small molecules, and modeling the breakdown diagram only requires the internal energy distribution of the neutral precursor.[8] Two assumptions are made when modeling the breakdown curve. First, the neutral internal energy distribution is transposed directly onto the ion manifold; in other words, the threshold ionization cross sections for sequence transitions are constant over the thermal energy range, and there is a uniform probability of threshold ionization across the neutral molecule's energy distribution.[8,9,13] The Franck−Condon factors for sequence transitions in small molecules at room temperature are dominated by rotational contributions, and this assumption will hold true as long as the geometries of the neutral and parent ion are sufficiently similar. However, it is important to note that no assumption is made about the Franck−Condon factors for threshold ionization as a function of photon energy. Second, the second integral in eq 2 assumes that zero internal energy neutrals always contribute to the parent ion signal. This is only valid if the ground state potential well is deep enough to accommodate the transposition of the entire thermal energy distribution of the neutral onto the ion manifold in the photon energy range of the breakdown diagram, which we term the "deep-well assumption" (Figure 1). However, if the width of
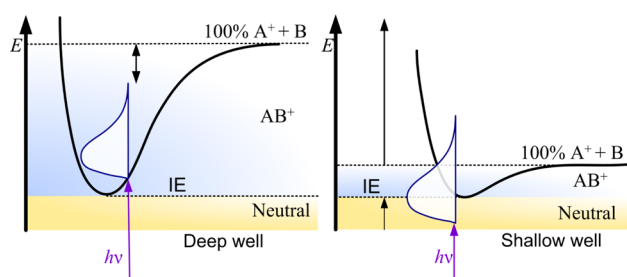
Figure 1. Schematic showing the deep well and the shallow well scenarios. As the photon energy ($h\nu$) is scanned, the parent ion (AB^+) fractional abundance corresponds to the normalized parent ion internal energy distribution integral from the bottom of the well to the barrier ($A^+ + B$). The daughter ion (A^+) factional abundance is given as the integral from the dissociation limit to infinity, and in the shallow well scenario, this integral is always non-negligible. For photon energies below the adiabatic IE, the breakdown diagram deviates from the shape predicted by the deep-well assumption, as the neutral thermal distribution cannot be fully incorporated onto the ionic manifold.

the thermal energy distribution is larger than the depth of the potential energy well, the low energy neutrals do not contribute to the ion signal. Now, the deep-well assumption is no longer valid, and what we term a "shallow-well reality" prevails. In such cases, the parent signal is always less than 100%, and there is significant daughter ion signal even at the ionization limit. This effect had been observed previously,[14] and was first discussed in the TPEPICO study of $CFBr_3$ and CBr_4.[7]

While a reasonable estimate for the 0 K onset can be trivially deduced for fast dissociations of small molecules, modeling the breakdown curve provides a more rigorous assessment of the assumptions, confidently confirming the shape and nature of the ion internal energy distribution and the validity of the deep well assumption. Even though the latter is applicable in most covalently bound ions, it is not always appropriate in weakly bound systems, a few of which we will examine in this work. In such cases, the adiabatic ionization energy (IE) can often be derived from the breakdown diagram.

As can be seen from eq 2, the modeled breakdown curves are temperature dependent, and the breakdown diagram is effectively a molecular thermometer, measuring the temperature of the neutral molecule. Additionally, oscillations or peaks in the breakdown curve, as was first observed for CH_3I^+,[6] may indicate changes in the threshold photoionization mechanism.
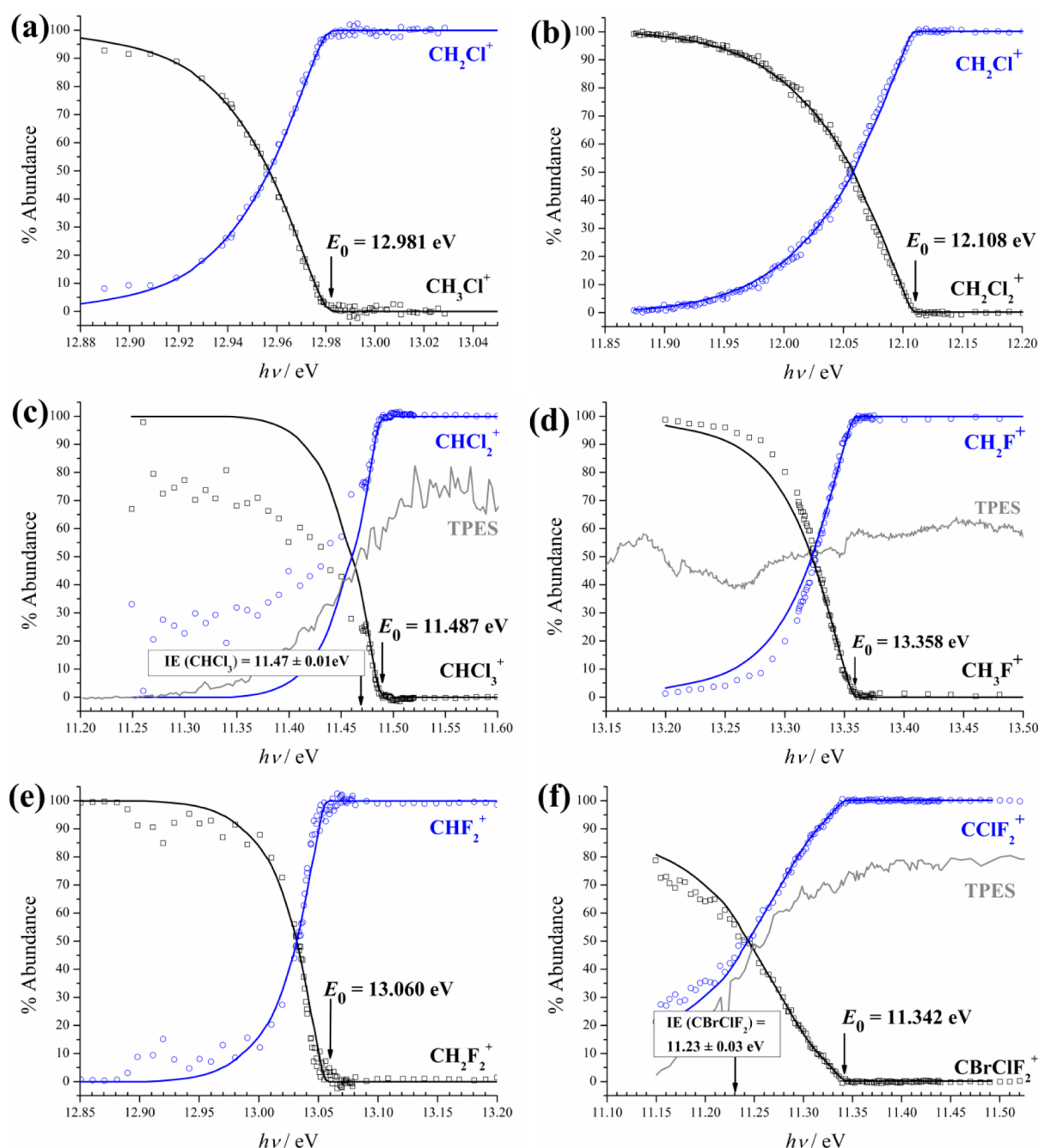
We employ calculations, together with experimental 0 K dissociative photoionization onsets, to derive a self-consistent thermochemical network, which links neutral and ionic species and provides improved enthalpies of formation, and reaffirms the results of previous theoretical and experimental studies.[3,15] Ion thermochemical values can be useful in the interpretation of ion dynamics, e.g., selected ion flow tube experiments.[16] Such self-consistent networks, similar to the active thermochemical tables of Ruscic et al.,[17] add to the expanding armamentarium of thermochemistry. The advantage of this approach over the purely ab initio route is that the network is pegged by the accurately measured onset energies and well-known enthalpies of formation such as those for CF_4 and CH_4, thus reducing the ab initio network plasticity and eliminating systematic errors. Such an approach has also been used to obtain updated enthalpies of formation for primary amines[18] as well as for bromofluoromethanes and their dissociative photoionization products.[7]

The products and reactants have equal numbers of the same types of bonds in isodesmic reactions.[19,20] It has been shown that these reactions yield reliable reaction energies, especially for closed shell species.[20,21] Quantum chemical calculations often suffer from error accumulation arising from basis set truncation, inaccuracies calculating valence electron correlation and zero-point vibrational energies,[22] and in heavier atoms, difficulty with accurate recovery of spin−orbit coupling effects.[1,5] These errors as well as relativistic and core correlation effects effectively cancel out in isodesmic reaction energy calculations.[19,20]

The lowest energy dissociative photoionization channel observed in the TPEPICO experiment corresponds to the cleavage of the weakest bond in the parent ion. Thus, with $CBrClF_2$ it is the C−Br bond that breaks first in dissociative photoionization to give $CClF_2^+$. In fully halogenated chlorofluoromethanes CCl_nF_{4-n} ($n = 1-3$), it is always a C−Cl bond that breaks first. When the halomethane molecule incorporates hydrogen atoms, the situation is not so clear-cut. For CH_3F and CH_2F_2, H-loss and cleavage of a C−H bond occurs at the lowest energy. Similarly, a C−H bond is the weakest and breaks at the lowest energy in CH_3Cl, whereas in the other two chloromethanes, CH_2Cl_2 and $CHCl_3$, a C−Cl bond breaks first. By contrast, the electronic ground state of the parent ion is repulsive in the Franck−Condon region in CCl_4, CF_4, and CHF_3.[23−25] Even though the accurate onset energy cannot be determined experimentally in these species, their neutral enthalpies of formation feature in the network through computed reaction energies. Two stand-alone compounds,

$CHClF_2$ and $CBrClF_2$, are also studied, which only connect to the rest of the network via their E_0 values as well as a neutral isodesmic reaction energy for the former. The dissociative photoionization of $CBrClF_2$ has, to the best of our knowledge, not been reported before, and its enthalpy of formation is not well-known. The experimental route is important here because reliable quantum chemical calculations involving bromine containing compounds are difficult to perform[26] due to the large numbers of electrons, and the fact that relativistic effects become significant for high-Z atoms.[15,27,28] Although Borkar et al. have found that relative energies of C_3H_5Br isomers can be quite well predicted by standard computational methods, too,[29] bromine- and iodine-containing species are omitted in the comprehensive study of Csontos et al.,[3] and Bodi et al. report large error bars, typically in the region of 7 kJ mol^{-1}, in a recent study on bromofluoromthanes.[7] The study of $CBrClF_2$ provides a link between bromine-containing species and the remainder of the lighter Cl and F containing species. We also seek to provide a more complete thermochemistry for the fragment ion CHF_2^+ by the dissociative photoionization of CH_2F_2 and $CHClF_2$, the latter of which has been studied before at inferior photon resolution using TPEPICO by Howle and co-workers.[30]

2. METHODS

2.1. Experimental Section. The imaging photoelectron photoion coincidence (iPEPICO) spectrometer at the X04DB beamline of the Swiss Light Source[31,32] has been described in detail elsewhere,[33] and only a brief overview is given here. The pure sample was introduced into the chamber through an effusive source at room temperature, with typical pressures in the experimental chamber being $2-4 \times 10^{-6}$ mbar during measurement. The background pressure is on the order of 10^{-7} mbar. The sample is ionized by incident monochromatic vacuum ultraviolet (VUV) synchrotron radiation dispersed by a grazing incidence monochromator. The effective photon energy resolution is 2 meV, and the photon energy is calibrated against the autoionization lines of argon in first and second order. Higher orders of radiation are removed using a compact Ne gas filter with an absorption path length of 10 cm, operating at 10 mbar pressure.

Following photoionization, the photoelectrons and photoions are accelerated in opposite directions by a constant extraction field of 120 V cm^{-1}. The photoelectrons are velocity map imaged onto a DLD40 Roentdek position-sensitive delay-line detector that has a kinetic energy resolution of better than 1 meV at threshold. A two-stage Wiley–McLaren time-of-flight mass spectrometer, for which the electron hits provide the "start" time, is used to mass select the ion fragments. Electron hit positions and times, together with the ion hits, are recorded in a triggerless mode of a HPTDC-PCI time-to-digital converter card and are correlated on the fly, in a multistart–multistep mode.[34] The hot electron contamination consists of kinetic energy electrons with a velocity vector orientated along the flight tube axis. Their contribution to the threshold signal in the detector center is accounted for by a subtraction process, as proposed by Sztáray and Baer.[35] The signal from a small ring around the central spot, as captured by the delay-line detector, is subtracted from the threshold signal. The large ion residence times in the first acceleration region lead to asymmetric peak shapes for unimolecular dissociation reactions with rate constants between 10^3 s^{-1} < k < 10^7 s^{-1}.[36] All dissociations probed in this paper are fast, producing symmetrical and narrow TOF peak shapes, indicating an absence of a kinetic shift.[37]

2.2. Computational Methods. Calculations were performed using Gaussian 09.[38] The dissociations were also confirmed to be fast by ab initio RRKM rate constant calculations at arbitrarily chosen transition state geometries along the dissociation coordinate. G3B3[39] and W1[40] composite methods were used to determine the neutral and ion energetics, which were used along with previously reported energies[3] in the construction of the thermochemical network shown in Figure 2.

Figure 2. The thermochemical network showing the experimental (E_0) and computational links. Enthalpies of formation are indicated as nodes. The appearance energies (straight dashed arrows) connect the neutrals with the ions; ab initio isodesmic (pairs of black curved links), $H_2/(F_2$ or $Cl_2)$, and F_2/Cl_2 exchange reactions (double headed arrows) connect neutral/neutral and ion/ion groups. Revised thermochemical values are indicated by dashed boxes. The absolute values of $\Delta_f H^\circ_{0K}$ are tethered to five anchor points: CH_4, CF_4, $CHCl_3$, CH_3^+ and CF_3^+.

Fast dissociative photoionization processes in threshold PEPICO experiments are modeled by taking into consideration the thermal energy distribution of the neutral molecule, which yields the energy distribution of the ion as a function of photon energy.[8] The experimental onset energies in the thermochemical network provide rigid links between the neutral and the ion enthalpies of formation. In the shallow well instances, the initial abundance of the first daughter ion is nonzero. Even in such cases, the fit was required to reproduce the disappearance energy range of the parent signal, thus giving the E_0 value. The photon energy, at which the deep well approximation fails, then yields the adiabatic IE.

3. RESULTS AND DISCUSSION

Before presenting the thermochemical network, we will first discuss the experimental results on the halogenated methanes according to their dissociative photoionization reactions 3a–3g:

$$CH_3Cl + h\nu \rightarrow CH_2Cl^+ + H + e^- \tag{3a}$$

$$CH_2Cl_2 + h\nu \rightarrow CH_2Cl^+ + Cl + e^- \tag{3b}$$

$$CHCl_3 + h\nu \rightarrow CHCl_2^+ + Cl + e^- \tag{3c}$$

$$CH_3F + h\nu \rightarrow CH_2F^+ + H + e^- \tag{3d}$$

$$CH_2F_2 + h\nu \rightarrow CHF_2^+ + H + e^- \tag{3e}$$

$$CHClF_2 + h\nu \rightarrow CHF_2^+ + Cl + e^- \tag{3f}$$

$$CBrClF_2 + h\nu \rightarrow CClF_2^+ + Br + e^- \tag{3g}$$

Figure 3. Breakdown diagram corresponding to (a) H loss in CH_3Cl^+, (b) Cl loss in $CH_2Cl_2^+$, (c) Cl loss in $CHCl_3^+$, (d) H loss in CH_3F^+, (e) H loss in $CH_2F_2^+$, and (f) Br loss in $CBrClF_2^+$. The experimental points (open shapes) are plotted together with the modeled breakdown curves (solid line). The derived 0 K onset energies are shown together with the new IEs for shallow-well parent ions $CHCl_3^+$ and $CBrClF_2^+$.

The potential well for the ground electronic states of $CHCl_3^+$, $CHClF_2^+$, and $CBrClF_2^+$ is quite shallow, enabling us to derive adiabatic IEs. The thermochemical network of the neutrals and ions incorporates the lowest energy dissociative photoionization channels obtained from the TPEPICO studies and calculated reaction energies. It is used to update 11 enthalpies of formation, including that for $CBrClF_2$. Several neutral and ion enthalpies of formation are also confirmed as reported in the literature.

3.1. Chlorinated Methanes. The breakdown diagram of CH_3Cl in the 12.88−13.05 eV photon energy range is shown in Figure 3a. The fitted E_0 for $CH_3Cl \rightarrow CH_2Cl^+ + H + e^-$, i.e., the 0 K appearance energy of the first daughter ion, is 12.981 ±

0.004 eV. Tang et al. also observed CH_2Cl^+ as the first daughter ion,[41] which is in contrast with photoionization by He(I) radiation at 21.2 eV, in which no CH_2Cl^+ was detected below 15 eV.[42,43] Autoionization is only possible in tunable VUV studies, such as this work. Because the H-loss channel opens up in a Franck−Condon gap, it is not accessible by direct photoionization, e.g., by using He(I) radiation, at threshold. On the other hand, the hydrogen "many-line" light source in an earlier tunable nonthreshold photoionization study by Werner et al.[44] may have provided insufficient flux around 13 eV for the H-loss channel to be observed.

The breakdown diagram of CH_2Cl_2 in the 11.85−12.20 eV photon energy range is shown in Figure 3b. The derived E_0 for

reaction 3b is 12.108 ± 0.003 eV. Our value is more accurate and somewhat lower than the 12.122 ± 0.010 eV reported by Lago et al.[45] obtained using a larger photon energy step size in the onset region. We note that both reactions 3a and 3b share a common fragment ion, CH_2Cl^+.

The breakdown diagram of $CHCl_3$ is given in Figure 3c across the 11.20−11.60 eV photon energy range. The fitted E_0 is 11.487 ± 0.005 eV. The $CHCl_2^+$ daughter ion is produced in reaction 3c, and its abundance at the literature IE of 11.3 eV[46] is nonzero, meaning that a significant proportion of parent ions have sufficient energy to dissociate, as was also reported by Shuman et al.[47] If the Franck−Condon factors for threshold ionization are assumed to be uniform across the thermal energy distribution, the breakdown curve may be modeled as the ratio of the integrated internal energy distribution *in* the potential well against that *above* the well. Because the portion of the distribution that falls below the IE does not contribute to the ion signal, the IE also influences the breakdown curve. Alternatively, instead of retro-fitting the IE to reproduce the breakdown curve, a deep potential well is assumed and the point at which the calculated curve deviates from the experimental curve can be taken as the adiabatic IE of the parent molecule. This was also the approach used in a study of $CFBr_3$ and CBr_4,[7] as well as for $C_2H_4I_2$,[14] where the point of deviation from the modeled curve led to a revised IE for these three molecules. In such cases, only initially hot neutrals are ionized at $h\nu$ < IE. Neutrals with less internal energy than (IE − $h\nu$) are not ionized, and the parent ion internal energy does not correspond to the Boltzmann distribution of the neutral in this energy range.[14] The advantage of using this method to determine the IE in such instances, as opposed to modeling the TPES by Franck−Condon simulations[48] or ab initio calculations, is its considerable ease of use. Furthermore, thanks to the enhanced resolution of the experiment, the deviation of the calculated fit and the experimental points at 11.47 ± 0.01 eV can clearly be seen, providing a new value for the IE of $CHCl_3$. As Figure 3c shows, the adiabatic IE is not easily identifiable from the threshold photoelectron spectrum (TPES) of the molecule, as the ground state of $CHCl_3^+$ is not vibrationally resolved, unlike that of CH_3Cl and CH_2Cl_2.[46] The signal onset for the ground state of the ion does appear to be 11.3 eV, which agrees with an 11.30 ± 0.05 eV appearance energy given by Seccombe et al.[49] from a lower-resolution TPEPICO study; they also quoted a vertical IE of 11.51 eV. Based on this latest breakdown diagram, we propose that the rise of the threshold electron signal below 11.47 eV is due to hot bands.

3.2. Fluorinated Methanes. Figure 3d shows the breakdown diagram of CH_3F in the 13.20−13.50 eV photon range. Two aspects are noted. First, the 0 K onset coincides with a small but sharp rise in the TPES signal. As was previously reported,[6] Rydberg state lifetime considerations, a proposed explanation for such rises, in the pulsed field ionization (PFI-) PEPICO experiments of methane[50] are unlikely to be at play in continuous field experiments. Consequently, this step function is probably due to an additional threshold photoionization channel that opens up at the onset and enhances daughter ion production. Second, and as a consequence of the first point, the whole breakdown curve cannot be faithfully modeled using a single temperature and the corresponding neutral internal energy distribution. The lower energy range, below 13.325 eV, is reproduced when 298 K is assumed while the parent ion abundances above the crossover are overestimated. A higher

temperature of 348 K models the higher energy points well but widens the breakdown diagram too much. However, it is the latter temperature that leads to a perfect fit in the most important energy region, namely at the disappearance energy of the parent signal. The fitted E_0 for reaction 3d is 13.358 ± 0.005 eV, much higher than the room temperature appearance energy (the photon energy at which daughter ion signal above the noise is first observed) quoted by Weitzel and co-workers as 13.20 ± 0.08 eV.[51] From their observed IE from the TPES of 12.53 eV and the 13.34 ± 0.02 eV crossover energy, they derived the dissociation energy of CH_3F^+ to be 0.84 ± 0.02 eV, and an E_0 of 13.37 ± 0.02 eV. They also reported a nonvanishing parent ion signal, i.e., one that does not decrease to 0% above the 0 K appearance energy. Our own crossover and onset energies are both ca. 20 meV lower. This discrepancy could result from insufficient hot electron suppression in the Weitzel study.

The breakdown diagram of CH_2F_2 in the 12.85−13.20 eV photon energy range is presented in Figure 3e. The fitted E_0 of reaction 3e is 13.060 ± 0.015 eV, with the larger error limit being a result of the curve having a small gradient near the E_0. This produces a tailing off of the parent signal, instead of a sharp cutoff. A possible reason for this and the slightly inferior signal-to-noise ratio at the onset energy compared with other molecules in this study may lie with the subtraction of the hot electron contamination. If the threshold electron yield is low at onset or changes quickly with photon energy, the ring area around the detector (which is subtracted from the center area signal) can be a poor representation of the hot electron background in the center. While the E_0 is independent of sample temperature, the shape of the curve at the onset is governed by it, and a softly landing parent ion curve leads to a less well-defined E_0. Using pulsed-field-ionization zero kinetic energy electrons (PFI-ZEKE), Forysinski et al. found the 0 K H-loss appearance energy to be 13.065 ± 0.003 eV.[52] This value from their laser-based very high-resolution study is 5 meV higher than our own reported value, but the two values are within the error limits. Both values are somewhat lower than the appearance energy of CHF_2^+ at 298 K of 13.08 ± 0.03 eV reported by Seccombe et al. from a lower resolution TPEPICO study.[53]

3.3. CBrClF_2 and CHClF_2. The breakdown diagram of $CBrClF_2$ in the 11.15−11.50 eV photon energy range along with the TPES is presented in Figure 3f. The C−Br bond is the weakest, and therefore the first dissociative photoionization channel produces $CClF_2^+$ + Br + $e^−$. The fitted E_0 value is 11.342 ± 0.003 eV. There is some ambiguity as to the adiabatic IE for $CBrClF_2$. The TPES has been studied several times, and vertical IEs of 11.51[54] and 11.83 eV[55] were reported. Another value for the IE is reported to be 11.21 eV, corresponding to the onset of the electron signal.[56] However, as can be seen from the TPES, the identification of the adiabatic IE is not immediately obvious. Similarly to $CHCl_3$ and $CHClF_2$, there is a significant daughter ion contribution of ca. 30% at the ionization onset. The modeled breakdown curve deviates from the experimental data points at a slightly higher energy of 11.23 ± 0.03 eV. We propose this somewhat higher value as the adiabatic IE of $CBrClF_2$. This fit is less sensitive to the assumed IE than for $CHCl_3$ and $CHClF_2$, as the deep well model only deviates at most over a few tens of millielectronvolts from the shallow-well reality.

The breakdown diagram of $CHClF_2$ (Figure 4) is shown in the 12.15−12.51 eV photon energy range, plotted together with
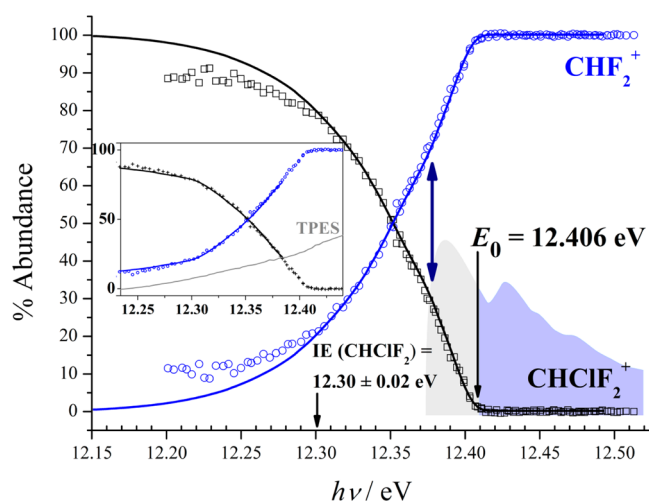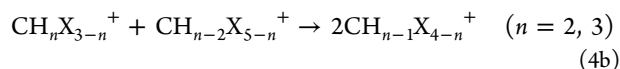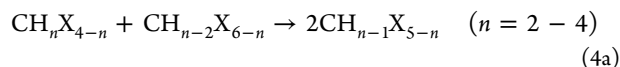
Figure 4. Breakdown diagram corresponding to Cl loss in the shallow well parent ion CHClF$_2^+$, along with the new IE of 12.30 ± 0.02 eV. The IE is hard to predict based on the broad featureless TPES shown in gray. The inset also shows breakdown diagram modeled with the new IE, where the lower $h\nu$ range is reproduced well by taking the actual potential energy well depth into account. The ion internal energy distribution at 12.37 eV is shown with parent contribution in gray and CClF$_2^+$ contribution in pale blue. The hump in the breakdown curve, indicated by a double-headed arrow at 12.37 eV, corresponds to an unusual minimum in the thermal energy distribution in the neutral, confirming the faithful transposition of internal energy distribution upon threshold photoionization.

the corresponding TPES. The C–Cl bond is the weakest, and the derived E_0 value for reaction 3g, the production of CHF$_2^+$, is 12.406 ± 0.004 eV. This is the same daughter ion as the first product from CH$_2$F$_2$. As with CHCl$_3$, there is significant daughter ion abundance present in the low energy region of the breakdown diagram, and the deep well approximation deviates from the experimental points over the range of 12.2−12.3 eV. This provides us with an accurate IE of 12.30 ± 0.02 eV, which is not easily determined from the TPES alone. The most recent IEs range from 12.15 ± 0.05 eV determined by TPES,[30] to 12.28 ± 0.02 eV determined by PIMS,[56] so our value is at the higher end of this range. Upon magnification, a small hump or bulge in the otherwise smooth breakdown curve becomes apparent at 12.37 eV. Interestingly, this feature is also faithfully reproduced by the model curves. To shed light on this peculiarity, we also plotted the calculated neutral thermal energy distribution in Figure 4, with its origin shifted to 12.37 eV. Two possible reasons have been suggested for such features in breakdown diagrams, namely, alternative photoionization mechanisms[6] or a less than faithful transposition of the neutral thermal energy distribution to the ion manifold.[8] Here, however, the explanation appears to be that the thermal energy distribution is indeed transposed onto the ion manifold, and we use our molecular thermometer to measure the Boltzmann distribution of neutral energies, which shows a dip at an internal energy of ca. 50 meV due to the higher density of rovibrational levels 15 meV higher.

3.4. Thermochemistry. In addition to the measured 0 K appearance energies, the neutral parents and daughter ions can be related to each other through a series of quantum chemical calculations involving closed-shell species as well, to generate the network shown in Figure 2. The neutral network is composed of three subnetworks: that of the chlorinated

methanes, the fluorinated methanes, and the chlorofluoro-methanes. Each subnetwork contains the independent iso-desmic reactions connecting the neutrals, e.g., CH$_n$X$_{4-n}$, as well as the ions, e.g., CH$_n$X$_{3-n}^+$, (X = F, Cl),

$$CH_nX_{4-n} + CH_{n-2}X_{6-n} \rightarrow 2CH_{n-1}X_{5-n} \quad (n = 2 - 4) \tag{4a}$$

$$CH_nX_{3-n}^+ + CH_{n-2}X_{5-n}^+ \rightarrow 2CH_{n-1}X_{4-n}^+ \quad (n = 2, 3) \tag{4b}$$

and the interconnecting exchange reactions for the ionic fragments where a new halomethane is generated by the substitution of a hydrogen with a halogen (e.g., H$_2$/X$_2$),

$$CH_nX_{3-n}^+ + \frac{1}{2}X_2 \rightarrow CH_{n-1}X_{4-n}^+ + \frac{1}{2}H_2$$

$$(n = 1 - 3) \tag{3c}$$
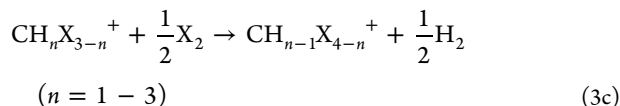
This approach was also adopted for the chlorofluoromethanes: CCl$_n$F$_{4-n}$ and CCl$_{n-1}$F$_{4-n}^+$.

The network is essentially a graph of vertices (enthalpies of formation of ions and neutrals) connected by edges. There are three types of edges: E_0 onset energies, neutral and ion isodesmic reaction energies, and exchange reaction energies (the latter only for fragment ions). The E_0 onset energies interconnect the neutral and ion groups, whereas the isodesmic and exchange reaction energies establish connections within the neutral and ion groups. If available, isodesmic reaction energies were obtained based on the energy values reported by Csontos et al.[3] Otherwise, W1 calculated reaction energies were used. G3B3 results were also obtained and checked for consistency. As a starting point in the optimization of the enthalpies of formation, the isodesmic, exchange, and dissociative photo-ionization reaction energies were also calculated using the literature $\Delta_f H^\circ_{0K}$ values.

The entire network needs to be tethered to an absolute scale of enthalpies of formation, and well-defined enthalpies of formation for a chosen set of species provide this vital link. These "anchor" enthalpies of formation are kept unchanged during the fitting process: $\Delta_f H^\circ_{0K}$ (CH$_4$) = −66.56 ± 0.06,[57] $\Delta_f H^\circ_{0K}$ (CF$_4$) = −927.8 ± 1.3,[3,57] $\Delta_f H^\circ_{0K}$ (CF$_3^+$) = 413.4 ± 2.0,[7] and $\Delta_f H^\circ_{0K}$ (CHCl$_3$) = −98.4 ± 1.1 kJ mol^{-1}.[58] The enthalpy of formation for CH$_3^+$ is derived from the 0 K onset energy for CH$_4$ + $h\nu$ → CH$_3^+$ + H + e$^-$, 14.323 ± 0.001 eV[59] combined with the H atom heat of formation, which yield $\Delta_f H^\circ_{0K}$(CH$_3^+$) = 1099.35 ± 0.1 kJ mol^{-1}, yet another anchor value. The two major groups of neutrals, the fluorinated methanes and chlorinated methanes, are "anchored" by CF$_4$/CH$_4$ and CHCl$_3$/CH$_4$, respectively. The chlorofluoromethane groups, CCl$_n$F$_{4-n}$ and CCl$_{n-1}$F$_{4-n}^+$, provide bridges between the chlorinated and the fluorinated methanes.

An overall error function (ε) is defined as the sum of component isodesmic, exchange, and experimental errors:

$$\varepsilon = \sum_i \varepsilon_i(\text{iso}) + \sum_j \varepsilon_j(\text{exc}) + \sum_k \varepsilon_k(\text{iPEPICO}) \tag{5}$$

where ε_i (iso) = $(\Delta_r H^\circ[\text{calc}]_{\text{iso}} - \Delta_r H^\circ[\Delta_f H^\circ]_{\text{iso}})^2$, ε_j(exc) = $(\Delta_r H^\circ[\text{calc}]_{\text{exc}} - \Delta_r H^\circ[\Delta_f H^\circ]_{\text{exc}})^2$, and ε_k(iPEPICO) = $(\Delta_r H^\circ[\text{meas}]_{\text{iPEPICO}} - \Delta_r H^\circ[\Delta_f H^\circ]_{\text{dissoc.photoionization}})^2$. $\Delta_r H^\circ[\text{calc}]$ are the reaction enthalpies at 0 K from ab initio calculations, and $\Delta_r H^\circ[\Delta_f H^\circ]$ are the enthalpy of formation based reaction enthalpies, the starting values for which are taken from the literature. The network is optimized by

Table 1. Derived and Literature Values for Enthalpies of Formation and Thermal Enthalpies, in Units of kJ mol^{-1}

species	$\Delta_f H^\circ_{0K}$	$\Delta_f H^\circ_{0K}$	$\Delta_f H^\circ_{298K}$ [a]	$H_{298K} - H_{0K}$ (W1)
CH$_4$		-66.56 ± 0.06 [c]	-74.55 ± 0.06 [c]	10.0
CH$_3$F		-228.5 ± 2.0 [d]	-236.9 ± 2.0 [d]	10.1 [d]
CH$_2$F$_2$		-442.6 ± 2.0 [d]	-450.5 ± 2.0 [d]	10.6 [d]
CHF$_3$		-687.7 ± 2.0 [d]	-694.9 ± 2.0 [d]	11.5 [d]
CF$_4$		-927.8 ± 1.3 [d]	-933.8 ± 1.3 [d]	12.8
CH$_3^+$		1099.35 ± 0.1 [e]	1095.60 ± 0.1 [e]	10.0
CH$_2$F$^+$	844.4 ± 2.1 [b]	837.0 [f]	840.4 ± 2.1 [b]	10.0
CHF$_2^+$	601.6 ± 2.7 [b]		598.4 ± 2.7 [b]	11.0
CF$_3^+$		413.4 ± 2.0 [g]	410.2 ± 2.0 [g]	11.1
CClF$_3$	-702.1 ± 3.5 [b]	-703.4 ± 3.1 [d]	-707.3 ± 3.5 [b]	13.7 [d]
CCl$_2$F$_2$	-487.8 ± 3.4 [b]	-487.9 ± 4.2 [d]	-492.1 ± 3.4 [b]	14.8 [d]
CCl$_3$F	-285.2 ± 3.2 [b]	-282.7 ± 5.3 [d]	-288.6 ± 3.2 [b]	15.9 [d]
CClF$_2^+$	552.2 ± 3.4 [b]		549.5 ± 3.4 [b]	11.8
CCl$_2$F$^+$	701.2 ± 3.3 [b]		699.0 ± 3.3 [b]	12.5
CH$_3$Cl		-74.3 ± 3.1 [d]	-82.6 ± 3.1 [d]	10.4 [d]
CH$_2$Cl$_2$		-88.66 ± 1.3 [h]	-95.7 ± 1.3 [h]	11.8 [d]
CHCl$_3$		-98.4 ± 1.1 [i]	-103.4 ± 1.1 [i]	14.1 [d]
CCl$_4$	-94.0 ± 3.2 [b]		-96.4 ± 3.2 [b]	17.1 [d]
CH$_2$Cl$^+$		961.1 ± 1.7 [j]	957.1 ± 1.7 [j]	10.1
CHCl$_2^+$	890.3 ± 2.2 [b]	891.7 ± 1.5 [k]	887.2 ± 2.2 [b]	11.3
CCl$_3^+$	849.8 ± 3.2 [b]	852.3 ± 2.5 [l]	848.3 ± 3.2 [b]	13.3
CBrClF$_2$	-446.6 ± 2.7 [b]	-423.8 ± 15 [m]	-457.6 ± 2.7 [b]	15.7 [n]
CHClF$_2$		-475.7 ± 3.1 [d]	-482.2 ± 3.1 [d]	12.3
Cl		119.6 [h]	121.3 [h]	6.28
F		77.3 [h]	79.4 [h]	6.5

[a]Conversion to 298 K is made using Chase NIST-JANAF compendium values for thermal enthalpies,[61] ($H_{298K} - H_{0K}$[C] = 1.05, $H_{298K} - H_{0K}$[H$_2$] = 8.47, $H_{298K} - H_{0K}$[F$_2$] = 8.82, $H_{298K} - H_{0K}$[Cl$_2$] = 9.18, and $H_{298K} - H_{0K}$[Br$_2$] = 24.5 kJ mol^{-1}). 298 K values for cations are obtained using the ion convention, $H_{298K} - H_{0K}$[e$^-$] = 0 kJ mol^{-1}. [b]This work. [c]Ruscic active thermochemical tables.[17] [d]Csontos et al. result confirmed by W1 calculation.[3] [e]Bodi et al.[6] [f]Lias et al.[63] [g]Bodi et al.[7] [h]Chase NIST-JANAF compendium.[61] [i]Manion.[58] [j]Lago et al.,[45] [k]Shuman et al.[62] [l]Hudgens et al.[66] [m]Burcat and Ruscic.[70] [n]G3B3 value.

minimizing this error function using the generalized reduced gradient method.[60]

Initially, the network is relaxed, and all enthalpies of formation except the anchor values are set as fit parameters. The exchange reaction error function is then weighted by 0.01 to make sure it influences the fit less than the isodesmic reaction errors, as the latter are more reliable. There are fewer experimental onset energies, which are also more accurate than the calculations. Therefore, the PEPICO error function is weighted by 100 to ensure its adequate representation in the optimization of the network. Thus, no data set overinfluences the outcomes. Next, by analyzing the optimized enthalpies of formation in the fully relaxed fit, we identified further literature values that could be kept constant in the fitting procedure. Notably, the enthalpies of formation reported by Csontos et al.[3] were compared with the optimized values. The average difference was found to be 0.05 kJ mol^{-1}, with a standard deviation of 0.77 kJ mol^{-1} and maximum of 1.35 kJ mol^{-1} for CH$_3$Cl, CH$_3$F, CH$_2$F$_2$, CHF$_3$, and CHClF$_2$.[3] These enthalpies of formation are, thus, confirmed as recommended by Csontos et al. and held constant in the final fit. Furthermore, the Chase value for $\Delta_f H^\circ_{0K}$ (CH$_2$Cl$_2$) = -88.66 ± 1.3 kJ mol^{-1} and the Lago value for $\Delta_f H^\circ_{0K}$ (CH$_2$Cl$^+$) = -961.1 ± 1.7 kJ mol^{-1} are kept unchanged.[45,61] The remaining enthalpies of formation for CH$_2$F$^+$, CHF$_2^+$, CClF$_2^+$, CCl$_2$F$^+$, CHCl$_2^+$, CCl$_3^+$, CF$_3$Cl, CF$_2$Cl$_2$, CFCl$_3$, CBrClF$_2$, and CCl$_4$ are the final fit parameters. The network is anchored to CF$_4$ on the left-hand side in Figure 2, but, since CCl$_4$ is a fit parameter, an alternative, asymmetric anchor is required for the chloromethane series. As the Manion

value for $\Delta_r H^\circ_{0K}$ (CHCl$_3$),[58] -98.4 ± 1.1 kJ mol^{-1}, has been used previously as an anchor value by Shuman et al.,[62] and has a lower error bar than the Csontos value of -94.6 ± 5.3 kJ mol^{-1}, we have also opted for it to act as anchor. Having established the anchor values, confirmed the most reliable literature enthalpies of formation that are also kept unchanged, and set the error function weights to construct a balanced fit, a final optimization was carried out to obtain the final results as summarized in Table 1.

Three sources determine the uncertainties of the final results: (1) the uncertainties in the anchor values that peg the network to the enthalpy of formation scale; (2) the calculation errors; and (3) the errors in the iPEPICO appearance energies. These were accounted for as follows: (1) the anchor values were set to the high and low limit of their confidence interval, and a relaxed fit was carried out establishing the network confidence interval for each optimized species; (2) a $\pm$ 2 kJ mol^{-1} uncertainty contribution was assumed for calculations; (3) a further ± 2 kJ mol^{-1} uncertainty contribution was assumed for species on which we have no direct experimental appearance energy data; (4) the iPEPICO appearance energy uncertainty was used otherwise. The confidence intervals listed in Table 1 are the result of these four contributions.

The conversion from 0 to 298 K is made by the relationship[61]

$$\Delta_f H_{298K} = \Delta_f H_{0K} + [H_{298K} - H_{0K}]_{\text{molecule}}$$
$$- [H_{298K} - H_{0K}]_{\text{constituent elements}} \tag{6}$$

The list of thermal enthalpies, $H_{298K} - H_{0K}$, is shown in Table 1. The W1 values are virtually identical to those from the Csontos et al. study.[3] The latter are used for the neutral molecules when available, but the G3B3 value is used for $CBrClF_2$. W1 values are used for the remaining neutrals and the fragment cations.

First, we consider data for the chlorinated and fluorinated methanes. The 0 K enthalpy of formation of CCl_3^+ is connected to the enthalpies of formation of CH_2Cl^+ and $CHCl_2^+$ via isodesmic and exchange pathways. Using well-established values for $\Delta_f H^{\circ}_{0K}(CHCl_3) = -98.4 \pm 1.1$ kJ mol^{-1},[58] and $\Delta_f H^{\circ}_{0K}(CH_2Cl_2) = -88.7 \pm 1.3$ kJ mol^{-1},[61] our global fit derives revised values for $\Delta_f H^{\circ}_{0K}(CHCl_2^+) = 890.3 \pm 2.2$ and $\Delta_f H^{\circ}_{0K}(CCl_3^+) = 849.8 \pm 3.2$ kJ mol^{-1}. The $CHCl_2^+$ value is similar to that determined by Shuman et al., 891.7 ± 1.5 kJ mol^{-1}.[62] The revised $\Delta_f H^{\circ}_{0K}(CCl_3^+)$ value is about 15 kJ mol^{-1} higher than the 834.6 kJ mol^{-1} quoted by Lias,[63] and an earlier value of Rodriguez and co-workers of 831.6 kJ mol^{-1}.[64] However, it agrees with the Robles et al. value of 847.68 ± 3.3 kJ mol^{-1} derived from $\Delta_f H^{\circ}_{0K}(CCl_3) = 69.8 \pm 2.5$ kJ mol^{-1} and their measured $IE(CCl_3) = 8.06 \pm 0.02$ eV.[65] It is also within the error limit of the Hudgens et al. value of $\Delta_f H^{\circ}_{0K}(CCl_3^+) = 852.3 \pm 2.5$ kJ mol^{-1}, also derived from photoionization of CCl_3.[66]

CH_2F^+ and CHF_2^+ are fitted parameters. They connect in the network to the fixed values of $\Delta_f H^{\circ}_{0K}$ of CH_3F, CH_2F_2, and $CHClF_2$ via their experimental 0 K appearance energies. We note that an experimental value for the enthalpy of formation of CH_3F has been surprisingly hard to determine, with Chase et al. quoting a value of -226 ± 33 kJ mol^{-1}.[61] One year earlier, Luo and Benson had recommended the "best" experimental value at 298 K to be -233.9 ± 4.2 kJ mol^{-1}, corresponding to -225.5 ± 4.2 kJ mol^{-1} at 0 K.[67] Given the importance and relative simplicity of this five-atom halogenated hydrocarbon, it is perhaps just as surprising that the range of theoretical values in the literature is also large. Values at 0 K from -224 to -230 kJ mol^{-1} have been reported by many authors, with errors spanning from ± 0.8 to ± 10.0 kJ mol^{-1}.[3,15,26,68-70] As explained above, we have fixed the 0 K value for CH_3F to that determined by Csontos et al., -228.5 ± 2.0 kJ mol^{-1}.[3] By contrast, the Chase and Csontos values for CH_2F_2 are almost equal, with similar errors of ca. ± 2.0 kJ mol^{-1}. The heat of formation of $CHClF_2$ is reported by Csontos et al. to be -475.7 ± 3.1 kJ mol^{-1},[3] with no obvious experimental value for comparison. The new value for $\Delta_f H^{\circ}_{0K}(CH_2F^+)$ of 844.4 ± 2.1 kJ mol^{-1} is significantly higher than that reported by Lias et al., 837.0 kJ mol^{-1}.[63] The new value for $\Delta_f H^{\circ}_{0K}(CHF_2^+)$, 601.6 ± 2.7 kJ mol^{-1}, is equivalent to 598.4 ± 2.7 kJ mol^{-1} at 298 K. This latter value is in reasonable agreement with a recent experimental value at 298 K from Seccombe et al. of 604 ± 3 kJ mol^{-1},[53,71] where the appearance energy at this temperature of CHF_2^+ from CH_2F_2 was corrected for thermal effects by the procedure of Traeger et al.[72]

Little is known about the enthalpy of formation of $CBrClF_2$; indeed, the only value we could find was -423.8 ± 15 kJ mol^{-1} given by Burcat.[70] As such, the heat of formation becomes a "fit" parameter, which is only connected to the network by the E_0 of the reaction $CBrClF_2 \rightarrow CClF_2^+ + Br + e^-$. Barring an overall reverse barrier, the result, $\Delta_f H^{\circ}_{0K}(CBrClF_2) = -446.6 \pm 2.7$ kJ mol^{-1}, falls just outside the generous error limit of the previous value.

The enthalpy of formation of CCl_4 given by Csontos et al. of -88.7 ± 6.4 kJ mol^{-1} lies toward the less negative end of the literature values and has the largest error limit among the values they derived.[3] We derive a revised more negative value for $\Delta_f H^{\circ}_{0K}$ of -94.0 ± 3.2 kJ mol^{-1}. This value is in excellent agreement with the Rodgers et al.[73] value of -93.7 ± 0.6 kJ mol^{-1} and the Chase value of -93.8 ± 2.1 kJ mol^{-1}.[61] We note that Csontos et al. seem to report more reliable enthalpies of formation for fluorine substituted methanes such as CHF_3, than when methane is substituted with multiple chlorine atoms such as in $CHCl_3$ and CCl_4.

Due to the lack of certainty regarding the enthalpies of formation of CCl_3F, CCl_2F_2, and $CClF_3$ in the literature, these values were also fitted. The resulting enthalpies are $\Delta_f H^{\circ}_{0K}(CCl_3F) = -285.2 \pm 3.2$, $\Delta_f H^{\circ}_{0K}(CCl_2F_2) = -487.8 \pm 3.4$ and $\Delta_f H^{\circ}_{0K}(CClF_3) = -702.1 \pm 3.5$ kJ mol^{-1}. These values are within the uncertainty limits of the Csontos et al. values, namely, -282.7 ± 5.3, -487.9 ± 4.2, and -703.4 ± 3.1 kJ mol^{-1}, respectively.[3] The Chase values of $\Delta_f H^{\circ}_{0K}(CCl_3F) = -285.5 \pm 6.3$ kJ mol^{-1} and $\Delta_f H^{\circ}_{0K}(CClF_3) = -702.8 \pm 3.3$ kJ mol^{-1} are also in close agreement with our results.[61] While there are no experimental results leading directly to CCl_2F^+ or $CClF_2^+$ in this work, their 0 K enthalpies of formation have been determined by isodesmic and exchange reaction energies to be 701.2 ± 3.3 and 552.2 ± 3.4 kJ mol^{-1}, respectively.

4. CONCLUSIONS

The thermochemistry of the halogenated methanes CH_3Cl, CH_2Cl_2, $CHCl_3$, CH_3F, CH_2F_2, $CHClF_2$, and $CBrClF_2$, and their fragment ions CH_2Cl^+, $CHCl_2^+$, CCl_3^+, CH_2F^+, CHF_2^+, CCl_2F^+, and $CClF_2^+$, was studied using a combination of experimental data from iPEPICO spectroscopy and ab initio calculations of isodesmic and exchange reaction energies. A thermochemical network was constructed, in which the neutral and ionic components were intraconnected by subnetworks of isodesmic and exchange reactions, and interconnected by the experimental 0 K dissociative photoionization energies. The network was anchored by the well-known enthalpies of formation for CF_4, CH_4, $CHCl_3$, CF_3^+ and CH_3^+. An error function was defined between measured dissociative photo-ionization onsets and calculated reaction energies on the one hand, and the reaction energies derived using the enthalpies of formation in the network vertices on the other. The optimum values for the enthalpies of formation were determined by minimizing this error function. This holistic approach has been successful in producing updated thermochemical values at 0 K for the neutrals CCl_4, $CBrClF_2$, $CClF_3$, CCl_2F_2, and CCl_3F, as -94.0 ± 3.2, -446.6 ± 2.7, -702.1 ± 3.5, -487.8 ± 3.4, and -285.2 ± 3.2 kJ mol^{-1}, respectively. Fitting the remaining neutral enthalpies of formation led to negligible changes. These selected values were held constant, and are therefore confirmed. Revised 0 K enthalpies of formation for the ions CH_2F^+, CHF_2^+, $CClF_2^+$, CCl_2F^+, $CHCl_2^+$ and CCl_3^+ have been determined as 844.4 ± 2.1, 601.6 ± 2.7, 552.2 ± 3.4, 701.2 ± 3.3, 890.3 ± 2.2 and 849.8 ± 3.2 kJ mol^{-1}, respectively. The adiabatic IEs can easily be obtained based on the breakdown diagram of weakly bound parent ions that only exist in a Franck–Condon-allowed shallow potential energy well. These have been found to be 11.47 ± 0.01 eV, 12.30 ± 0.02 eV, and 11.23 ± 0.03 eV for $CHCl_3$, $CHClF_2$, and $CBrClF_2$, respectively. We suggest that this is the experimental method of choice to determine the IE of molecules where the ground state of the parent ion is only weakly bound. Finally, because of an uncharacteristic dip in the density of states, the thermal energy distribution of $CHClF_2$ shows a minimum at 50 meV.

This interesting feature is also seen and modeled as a small hump at 12.37 eV in the otherwise smooth breakdown curve for $CHClF_2^+$.

ASSOCIATED CONTENT

Supporting Information

Computed energies and details of the thermochemical network and the fits are available as Supporting Information. This material is available free of charge via the Internet at http://pubs.acs.org.

AUTHOR INFORMATION

Corresponding Author

*E-mail: r.p.tuckett@bham.ac.uk (R.P.T.); andras.boedi@psi.ch (A.B.).

Notes

The authors declare no competing financial interest.

ACKNOWLEDGMENTS

REFERENCES

(1) Peterson, K. A.; Feller, D.; Dixon, D. A. *Theor. Chem. Acc.* **2012**, *131*, 1079–1099.

(2) Karton, A.; Daon, S.; Martin, J. M. L. *Chem. Phys. Lett.* **2011**, *510*, 165–178.

(3) Csontos, J.; Rolik, Z.; Das, S.; Kállay, M. *J. Phys. Chem. A* **2010**, *114*, 13093–13103.

(4) Feller, D.; Peterson, K. A.; Dixon, D. A. *J. Phys. Chem. A* **2011**, *115*, 1440–1451.

(5) Feller, D.; Peterson, K. A.; Grant Hill, J. *J. Chem. Phys.* **2011**, *135*, 044102–044120.

(6) Bodi, A.; Shuman, N. S.; Baer, T. *Phys. Chem. Chem. Phys.* **2009**, *11*, 11013–11021.

(7) Bodi, A.; Kvaran, Á.; Sztáray, B. *J. Phys. Chem. A* **2011**, *115*, 13443–13451.

(8) Sztáray, B.; Bodi, A.; Baer, T. *J. Mass Spectrom.* **2010**, *45*, 1233–1245.

(9) Borkar, S.; Sztáray, B. *J. Phys. Chem. A* **2010**, *114*, 6117–6123.

(10) Boese, A. D.; Oren, M.; Atasoylu, O.; Martin, J. M. L.; Kállay, M.; Gauss, J. *J. Chem. Phys.* **2004**, *120*, 4129–4142.

(11) Tajti, A.; Szalay, P. G.; Császár, A. G.; Kállay, M.; Gauss, J.; Valeev, E. F.; Flowers, B. A.; Vázquez, J.; Stanton, J. F. *J. Chem. Phys.* **2004**, *121*, 11599–11613.

(12) Baer, T.; Sztáray, B.; Kercher, J. P.; Lago, A. F.; Bodi, A.; Skull, C.; Palathinkal, D. *Phys. Chem. Chem. Phys.* **2005**, *7*, 1507–1513.

(13) Kercher, J. P.; Stevens, W.; Gengeliczki, Z.; Baer, T. *Int. J. Mass. Spectrom.* **2007**, *267*, 159–166.

(14) Baer, T.; Walker, S. H.; Shuman, N. S.; Bodi, A. *J. Phys. Chem. A* **2012**, *116*, 2833–2844.

(15) Lazarou, Y. G.; Papadimitriou, V. C.; Prosmitis, A. V.; Papagiannakopoulos, P. *J. Phys. Chem. A* **2002**, *106*, 11502–11517.

(16) Simpson, M. J.; Tuckett, R. P. *J. Phys. Chem. A* **2012**, *116*, 8119–8129.

(17) Ruscic, B. Active Thermochemical Tables, early beta 1.110, http://atct.anl.gov/index.html, May 09, 2012.

(18) Bodi, A.; Kercher, J. P.; Bond, C.; Meteesatien, P.; Sztáray, B.; Baer, T. *J. Phys. Chem. A* **2006**, *110*, 13425–13433.

(19) Wheeler, S. E.; Houk, K. N.; Schleyer, P. v. R.; Allen, W. D. *J. Am. Chem. Soc.* **2009**, *131*, 2547–2560.

(20) Wodrich, M. D.; Corminboeuf, C.; Wheeler, S. E. *J. Phys. Chem. A.* **2012**, *116*, 3436–3447.

(21) Raghavachari, K.; Stefanov, B. B.; Curtiss, L. A. *J. Chem. Phys.* **1997**, *106*, 6764–6767.

(22) Feller, D.; Peterson, K. A.; Dixon, D. A. *J. Chem. Phys.* **2008**, *129*, 204105–204136.

(23) Smith, D. M.; Tuckett, R. P.; Yoxall, K. R.; Codling, K.; Hatherly, P. A. *Chem. Phys.* **1993**, *216*, 493–502.

(24) Simm, I. G.; Danby, C. J.; Eland, J. H. D.; Mansell, P. I. *J. Chem. Soc., Faraday Trans. 2* **1976**, *72*, 426–434.

(25) Parkes, M. A.; Chim, R. Y. L.; Mayhew, C. A.; Mikhailov, V. A.; Tuckett, R. P. *Mol. Phys.* **2006**, *104*, 263–272.

(26) Feller, D.; Peterson, K. A.; Jong, W. A. d.; Dixon, D. A. *J. Chem. Phys.* **2003**, *118*, 3510–3522.

(27) Dixon, D. A.; Grant, D. J.; Christe, K. O.; Peterson, K. A. *Inorg. Chem.* **2008**, *47*, 5485–5494.

(28) Grant, D. J.; Garner, E. B.; Matus, M. H.; Nguyen, M. T.; Peterson, K. A.; Francisco, J. S.; Dixon, D. A. *J. Phys. Chem. A* **2010**, *114*, 4254–4265.

(29) Borkar, S. N.; Sztáray, B.; Bodi, A. *Int. J. Mass Spectrom.* **2012**, DOI: 10.1016/j.ijms.2012.08.014.

(30) Howle, C. R.; Collins, D. J.; Tuckett, R. P.; Malins, A. E. R. *Phys. Chem. Chem. Phys.* **2005**, *7*, 2287–2297.

(31) Johnson, M.; Bodi, A.; Schulz, L.; Gerber, T. *Nucl. Instrum. Methods Phys. Res. A* **2009**, *610*, 597–603.

(32) Bodi, A.; Hemberger, P.; Gerber, T.; Sztáray, B. *Rev. Sci. Instrum.* **2012**, *83*, 083105.

(33) Bodi, A.; Johnson, M.; Gerber, T.; Gengeliczki, Z.; Sztáray, B.; Baer, T. *Rev. Sci. Instrum.* **2009**, *80*, 034101.

(34) Bodi, A.; Sztáray, B.; Baer, T.; Gerber, T.; Johnson, M. *Rev. Sci. Instrum.* **2007**, *78*, 084102.

(35) Sztáray, B.; Baer, T. *Rev. Sci. Instrum.* **2003**, *74*, 3763–3768.

(36) Harvey, J.; Bodi, A.; Tuckett, R. P.; Sztáray, B. *Phys. Chem. Chem. Phys.* **2012**, *14*, 3935–3948.

(37) Chupka, W. A. *J. Chem. Phys.* **1959**, *30*, 191–211.

(38) Frisch, M. J. et al. *Gaussian 09*, revision A.1; Gaussian, Inc.: Wallingford CT, 2009.

(39) Baboul, A. G.; Curtiss, L. A.; Redfern, P. C.; Raghavachari, K. J. *J. Chem. Phys.* **1999**, *110*, 7650–7657.

(40) Martin, J. M. L.; de Oliveira, G. *J. Chem. Phys.* **1999**, *111*, 1843–1856.

(41) Tang, X.; Zhou, X.; Wu, M.; Liu, S.; Liu, F.; Shan, X.; Sheng, L. *J. Chem. Phys.* **2012**, *136*, 034304–034312.

(42) Lane, I. C.; Powis, I. *J. Phys. Chem.* **1993**, *97*, 5803–5808.

(43) Eland, J. H. D.; Frey, R.; Kuestler, A.; Schulte, H.; Brehm, B. *Int. J. Mass. Spectrom. Ion Phys.* **1976**, *22*, 155–170.

(44) Werner, A. S.; Tsai, B. P.; Baer, T. *J. Chem. Phys.* **1974**, *60*, 3650–3657.

(45) Lago, A. F.; Kercher, J. P.; Bodi, A.; Sztáray, B.; Miller, B.; Wurzelmann, D.; Baer, T. *J. Phys. Chem. A* **2005**, *109*, 1802–1809.

(46) Von Niessen, W.; Åsbrink, L.; Bieri, G. *J. Electron Spectrosc. Relat. Phenom.* **1982**, *26*, 173–201.

(47) Schuman, N.; Zhao, L. Y.; Boles, M.; Baer, T.; Sztáray, B. *J. Phys. Chem. A* **2008**, *112*, 10533–10538.

(48) Innocenti, F.; Eypper, M.; Lee, E. P. F.; Stranges, S.; Mok, D. K. W.; Chau, F.-t.; King, G. C.; Dyke, J. M. *Chem.—Eur. J.* **2008**, *14*, 11452–11460.

(49) Seccombe, D. P.; Chim, R. Y. L.; Jarvis, G. K.; Tuckett, R. P. *Phys. Chem. Chem. Phys.* **2000**, *2*, 769–780.

(50) Weitzel, K.-M.; Jarvis, G. K.; Malow, M.; Baer, T.; Song, Y.; Ng, C. Y. *Phys. Rev. Lett.* **2001**, *86*, 3526–3529.

(51) Weitzel, K.-M.; Güthe, F.; Mähnert, J.; Locht, R.; Baumgärtel, H. *Chem. Phys.* **1995**, *201*, 287–298.

(52) Forysinski, P. W.; Zielke, P.; Luckhaus, D.; Signorell, R. *Phys. Chem. Chem. Phys.* **2010**, *12*, 3121−3130.

(53) Seccombe, D. P.; Tuckett, R. P.; Fisher, B. O. *J. Chem. Phys.* **2001**, *114*, 4074−4088.

(54) Cvitaš, T.; Klasinc, L.; Novak, I. *Int. J. Quantum Chem.* **1980**, *18*, 305−313.

(55) Doucet, J.; Gilbert, R.; Sauvageau, P.; Sandorfy, C. *J. Chem. Phys.* **1975**, *62*, 366−369.

(56) Lias, S. G.; Bartmess, J. E.; Liebman, J. F.; Holmes, J. L.; Levin, R. D.; Mallard, W. G. "Ion Energetics Data". In *NIST Chemistry WebBook, NIST Standard Reference Database Number 69*; Linstrom, P. J., Mallard, W. G., Eds.; National Institute of Standards and Technology: Gaithersburg MD, 2005.

(57) Ruscic, B. Active Thermochemical Tables, early beta 1.110, 2012.

(58) Manion, J. A. *J. Phys. Chem. Ref. Data.* **2002**, *31*, 124−165.

(59) Weitzel, K.-M.; Malow, M.; Jarvis, G. K.; Baer, T.; Song, Y.; Ng, C. Y. *J. Chem. Phys.* **1999**, *111*, 8267−8270.

(60) Lasdon, L. S.; Waren, A. D. *Generalized Reduced Gradient −2 User's Guide (As Implemented in the Excell Program)*; School of Business Administration, University of Texas at Austin: Austin, TX, 1986.

(61) Chase, M. W. *J. Phys. Chem. Ref. Data., Monograph 9* **1998**, 1−1951.

(62) Shuman, N.; Zhao, L. Y.; Boles, M.; Baer, T.; Sztáray, B. *J. Phys. Chem. A.* **2008**, *112*, 10533−10538.

(63) Lias, S. G.; Bartmess, J. E.; Liebman, J. F.; Holmes, J. L.; Levin, R. D.; Mallard, W. G. *J. Phys. Chem. Ref. Data.* **1988**, *17*.

(64) Rodriquez, C. F.; Bohme, D. K.; Hopkinson, A. C. *J. Phys. Chem.* **1996**, *100*, 2942−2949.

(65) Robles, E. S. J.; Chen, P. *J. Phys. Chem.* **1994**, *98*, 6919−6923.

(66) Hudgens, J. W.; Johnson, R. D. I.; Timonen, R. S.; Seetula, J. A.; Gutman, D. *J. Phys. Chem.* **1991**, *95*, 4400−4405.

(67) Luo, Y. R.; Benson, S. W. *J. Phys. Chem. A* **1997**, *101*, 3042−3044.

(68) Berry, R. J.; Burgess, D. R. F.; Nyden, M. R.; Zachariah, M. R. *J. Phys. Chem. A* **1995**, *99*, 17145−17150.

(69) Kormos, B. L.; Liebman, J. F.; Cramer, C. J. *J. Phys. Org. Chem.* **2004**, *17*, 656−664.

(70) Burcat, A.; Ruscic, B. September 2005 Third Millennium Ideal Gas and Condensed Phase Thermochemical Database for Combustion with Updates from Active Thermochemical Tables, ANL-05/20 and TAE 960, Technion-IIT; Aerospace Engineering, and Argonne National Laboratory, Chemistry Division, September 2011. ftp://ftp.technion.ac.il/pub/supported/aetdd/thermodynamics.

(71) Zhou, W.; Seccombe, D. P.; Tuckett, R. P.; Thomas, M. K. *Chem. Phys.* **2002**, *283*, 419−431.

(72) Traeger, J. C.; McLoughlin, R. G. *J. Am. Chem. Soc.* **1981**, *103*, 3647−3652.

(73) Rodgers, A. S.; Chao, J.; Wilhoit, R. C.; Zwolinski, B. J. *J. Phys. Chem. Ref. Data* **1974**, *3*, 117−140.